AIP Journal of Applied Physics

Evidence for boron diffusion into sub-stoichiometric MgO (001) barriers in CoFeB/MgO-based magnetic tunnel junctions

V. Harnchana, A. T. Hindmarch, M. C. Sarahan, C. H. Marrows, A. P. Brown, and R. M. D. Brydson

Citation: Journal of Applied Physics **113**, 163502 (2013); doi: 10.1063/1.4802692
View online: http://dx.doi.org/10.1063/1.4802692
View Table of Contents: http://scitation.aip.org/content/aip/journal/jap/113/16?ver=pdfcov
Published by the AIP Publishing

Articles you may be interested in
Effects of boron composition on tunneling magnetoresistance ratio and microstructure of CoFeB/MgO/CoFeB pseudo-spin-valve magnetic tunnel junctions
J. Appl. Phys. **111**, 043913 (2012); 10.1063/1.3688039

Boron diffusion in magnetic tunnel junctions with MgO (001) barriers and CoFeB electrodes
Appl. Phys. Lett. **96**, 262501 (2010); 10.1063/1.3457475

MgO barrier-perpendicular magnetic tunnel junctions with CoFe/Pd multilayers and ferromagnetic insertion layers
Appl. Phys. Lett. **95**, 232516 (2009); 10.1063/1.3265740

Effect of Ta getter on the quality of MgO tunnel barrier in the polycrystalline Co Fe B Mg O Co Fe B magnetic tunnel junction
Appl. Phys. Lett. **90**, 012505 (2007); 10.1063/1.2426902

Compositional change of MgO barrier and interface in Co Fe B Mg O Co Fe B tunnel junction after annealing
J. Appl. Phys. **99**, 08T316 (2006); 10.1063/1.2170591

AIP Journal of Applied Physics

Journal of Applied Physics is pleased to announce André Anders as its new Editor-in-Chief

[This article is copyrighted as indicated in the article. Reuse of AIP content is subject to the terms at: http://scitation.aip.org/termsconditions. Downloaded to] IP: 129.234.252.65 On: Wed, 09 Jul 2014 08:47:52

JOURNAL OF APPLIED PHYSICS 113, 163502 (2013)

Evidence for boron diffusion into sub-stoichiometric MgO (001) barriers in CoFeB/MgO-based magnetic tunnel junctions

V. Harnchana,[1,2,4,a)] A. T. Hindmarch,[2,b)] M. C. Sarahan,[3] C. H. Marrows,[2] A. P. Brown,[1] and R. M. D. Brydson[1]

[1]*Institute for Materials Research, School of Process, Environmental and Materials Engineering, University of Leeds, Leeds LS2 9JT, United Kingdom*
[2]*School of Physics and Astronomy, University of Leeds, Leeds LS2 9JT, United Kingdom*
[3]*EPSRC UK National SuperSTEM Facility for Aberration-corrected STEM, Daresbury Laboratories, Warrington WA4 4AD, United Kingdom*
[4]*Department of Physics, Faculty of Science, Khon Kaen University, Khon Kaen 40002, Thailand*

(Received 27 February 2013; accepted 8 April 2013; published online 23 April 2013)

Evidence of boron diffusion into the MgO barrier of a CoFeB/MgO based magnetic tunnel junction has been identified using analytical scanning transmission electron microscopy (STEM) and X-ray photoelectron spectroscopy. Structures were deposited by DC/RF-magnetron sputtering, where defective, sub-stoichiometric MgO barriers degrading device performance have been previously mitigated against by deposition of thin Mg layers prior to MgO deposition. We show that despite the protection offered by the Mg layer, disorder in the MgO barrier is still evident by STEM analysis and is a consequence of the oxidation of the $Co_{40}Fe_{40}B_{20}$ surface during MgO deposition. Evidence of boron diffusion from CoFeB into the MgO barrier in the as-deposited and annealed structure is also presented, which in the as-deposited case we suggest results from the defective structures at the barrier interfaces. Annealing at 375 °C results in the presence of B in the trigonal coordination of $[BO_3]^{3-}$ in the MgO barrier and partial crystallization of the top electrode (we presume there is also some boron diffusion into the Ta capping layer). The bottom electrode, however, fails to crystallize and much of the boron is retained in this thicker electrode. A higher annealing temperature or lower initial boron content is required to crystallize the bottom electrode.
© *2013 AIP Publishing LLC* [http://dx.doi.org/10.1063/1.4802692]

I. INTRODUCTION

Coherent lattice matching at the interfaces of the electrode and the barrier in a CoFeB/MgO based magnetic tunnel junction (MTJ) has been established as a prerequisite for a large tunneling magnetoresistance (TMR).[1] A high TMR ratio has been reported from an epitaxial system of CoFe(100)[110]/MgO(100)[100]/CoFe(100)[110] after annealing at high temperature.[2] Experimental TMRs as high as 604% at room temperature have been reported so far,[3] which result from the deposition of the MgO barrier onto amorphous CoFeB electrodes and stabilization of a fully epitaxial and defect-free MgO tunnel barrier that is obtained after post-annealing to crystallize the CoFeB. In practice, growing such a high quality MgO barrier is dependent on the deposition technique used and is particularly challenging for sputter-deposited systems since sputtering MgO onto a CoFeB electrode tends to introduce oxidation and the formation of defects and disorder at the interface and/or inside the MgO barrier.[4] Cha *et al.*[5] have demonstrated that MgO barriers produced by RF sputtering contain significant amounts of defects compared to those prepared by electron beam evaporation. Despite this problem, DC or RF sputtering is still widely used in many research groups and industries because of its potential production rate. In this paper, we shall investigate magnetic tunnel junctions with a tunnel barrier composition of $Co_{40}Fe_{40}B_{20}$-MgO-$Co_{40}Fe_{40}B_{20}$ fabricated using a DC-RF magnetron sputtering system. We have shown previously that this system results in the deposition of disordered and sub-stoichiometric MgO crystallites embedded in an amorphous matrix and that this is due to the oxidation of the bottom CoFeB electrode during the MgO deposition.[6] To partially mitigate against this oxidation, we produced the MgO barriers reported here by depositing an ultra-thin Mg layer (one unit cell) prior to the deposition of MgO.[7]

This paper will provide a thorough structural study of the CoFeB/MgO based MTJ using a combination of scanning transmission electron microscopy (STEM) imaging and spatially resolved electron energy loss spectrometry (EELS). This will be correlated with data from time resolved X-ray photoelectron spectroscopy (XPS) of bilayer junctions recorded during depth profiling induced by *in-situ* Ar^+ ion sputtering. Key to this work is the analysis of boron following deposition and annealing which currently attracts a great deal of interest. CoFeB deposition typically results in a smooth, amorphous electrode layer (upon which oriented, crystalline MgO can be deposited) and to enhance the TMR of such a structure, it is then necessary to anneal it in order to drive the boron atoms out of the electrode and crystallize bcc CoFe to provide a coherent interface with the MgO.[8]

[a)]Author to whom correspondence should be addressed. Electronic mail: viyada@kku.ac.th
[b)]Present address: Department of Physics, University of Durham, Durham DH1 3LE, United Kingdom.

 © 2013 AIP Publishing LLC

[This article is copyrighted as indicated in the article. Reuse of AIP content is subject to the terms at: http://scitation.aip.org/termsconditions. Downloaded to] IP: 129.234.252.65 On: Wed, 09 Jul 2014 08:47:52

The resulting distribution of B in the CoFeB and MgO layers plus that in any B-scavenging capping layers (such as Ta) is critical to the performance of the device.[9]

You *et al*. proposed that upon annealing, boron diffuses toward the MgO layer forming boron oxide at the MgO/CoFeB interfaces, with the reasoning that it is unlikely to dissolve inside the MgO barrier due to a valence mismatch.[10] These findings were similar to the XPS study by Bae *et al*.,[11] where boron oxide (B_2O_3) was found to form near the interface and was thought to arise due to the presence of excess oxygen at the interface as well as from boron atoms that may have diffused out of the electrode towards the MgO barrier during deposition. More recently, Greer *et al*.[12] have quantified the boron distribution for a $Ta/Co_{20}Fe_{60}B_{20}/MgO$ sample annealed at 300 °C, indicating ~20% of the boron diffuses into the MgO and ~20% into a thin TaB interface layer. Han *et al*.[13] identified metallic boron, some oxidized boron, and an intermediate phase in an as deposited CoFeB top electrode and also identify B_2O_3 in the MgO barrier upon annealing.[14] Kodzuka *et al*.[15] show that the CoFeB crystallization (and consequent TMR values) depends on the boron content as well as the annealing temperature, with a higher boron content electrode $[(Co_{25}Fe_{75})_{67}B_{33}]$ inhibited from full crystallization even after annealing at 450 °C because of the metalloid stabilization of the CoFeB phase and insufficient out-diffusion of the boron. Clearly, the structure of the interfaces is crucial for the TMR performance and a particularly sensitive probe of structure is STEM high angle annular dark field (HAADF) imaging (in which the image contrast and intensity is related to the atomic column orientation [channeling] and atomic number of the elements within the specimen [Z-contrast]).[16] A significant outcome of the present work is that HAADF-STEM imaging appears to be more sensitive to the presence of interfacial disorder than phase contrast (S)TEM and this disorder may have important implications for the mobility of boron in such structures.

II. EXPERIMENTAL DETAIL

MTJs with a stack sequence of Si(100) substrate with 100 nm thermal oxide coating /Ta[3]/Ru[30]/Ta[3]/CoFeB[4]/MgO[3]/CoFeB[2.5]/Ru[1.5]/NiFe[4]/IrMn[20]/Ta[3]/Ru[4] (where figures inside the [] brackets are the layer thickness in nm were fabricated using a DC-RF magnetron sputtering system with a base pressure better than 3×10^{-8} Torr. The CoFeB, deposited from a $Co_{40}Fe_{40}B_{20}$ alloy target, was DC-magnetron sputtered as were all other metal layers in the structure. In contrast, the MgO barrier was deposited from a sintered MgO target using RF magnetron sputtering after the deposition of an ultrathin Mg layer (one unit cell thick) by DC-magnetron sputtering.[7] The MTJs were annealed at 375 °C in a separate vacuum furnace with a base pressure of 10^{-6} Torr with no applied magnetic field for a period of 1 h.

The samples for STEM analysis were prepared by a conventional TEM cross-section route: mechanical grinding and Ar+ ion milling using a Gatan precision ion polishing system. HAADF-STEM imaging and EELS were carried out with a VG-HB501 STEM fitted with a Nion C_s corrector. The instrument is equipped with a cold field emission filament operating at 100 kV (energy spread 0.3 eV) and a Gatan Enfina electron energy loss spectrometer with a dispersion setting of 0.2 eV/ch. The electron beam convergence semi-angle was 24 mrad and the collection semi-angle for EELS was 19 mrad. The HAADF detector was used for incoherent imaging, with a collection semi-angle range of 70–210 mrad. The bright field detector was used for phase contrast imaging, with a collection angle up to 6 mrad. The medium angle annular dark field (MAADF) detector was used for mixed contrast dark field imaging, with a convergence semi-angle range of 35–100 mrad. The minimum focused probe diameter obtained with this microscope is 0.91 Å with a measured current at the specimen of 100 pA.

XPS depth profile analysis was performed on bilayer CoFeB[4]/Mg + MgO[3] structures with ~1 nm Ta capping layer using a VG ESCAlab 250 photoelectron spectrometer with a monochromated Al Kα X-ray source. Depth profiling was achieved using 3 keV Ar+ ion etching with a beam current of 1 μA and beam raster scanned over 3 mm × 3 mm on the sample.

III. RESULTS AND DISCUSSION

A. The as-deposited structure

MAADF STEM reveals that the MgO barrier contains crystallites exhibiting (200) lattice fringes consistent with (100) texture at the middle of the barrier layer [Fig. 1(a)]. At both interfaces, low intensity, disordered, or amorphous layers are evident. The lack of MgO crystallinity at the interfaces is significantly more evident in the HAADF images [Fig. 1(b) and its magnified image Fig. 1(c)]; presumably, this arises from the requirement for channeling to form STEM HAADF atomic column images, with any disorder disrupting the channeling and so deteriorating the atomic column visibility.[17] In addition to channeling contrast, intensity in HAADF images varies as approximately $Z^{1.7}$, where Z is the average atomic number, suggesting that there could also be a different composition at the interfaces resulting, for example, from boron enrichment [Figs. 1(b) and 1(c)]. However, the lack of an apparent lattice in both MAADF and HAADF images in some regions of the MgO barrier indicates that here, atomic disorder dominates the structure. It has already been suggested that these disordered regions form because of a high defect density concurrent with sub-stoichiometry and this explanation is consistent with the apparent change in shape of oxygen *K*-edge electron loss spectra taken from the top and bottom of the CoFeB/MgO interfaces.[6] Specifically, pre-peaks in the oxygen *K*-edge EELS at ca. 530 eV energy loss [Figs. 1(d) and 1(e)] are characteristic of metals oxides containing gap states due to oxygen vacancies.[18] These pre-peaks are accompanied by a much more evident reduction in the relative intensity, broadening, and associated shift in the energy of the peak maximum of the main energy loss peak of the oxygen *K*-edge, centred at 535-540 eV and is presumed to result from a reduction in medium and long range order in the oxygen sub-lattice.[17] Both these spectral changes are more evident at the bottom interface. The composition of this amorphous oxide layer may also be critical to the device's function and we

[This article is copyrighted as indicated in the article. Reuse of AIP content is subject to the terms at: http://scitation.aip.org/termsconditions. Downloaded to] IP: 129.234.252.65 On: Wed, 09 Jul 2014 08:47:52

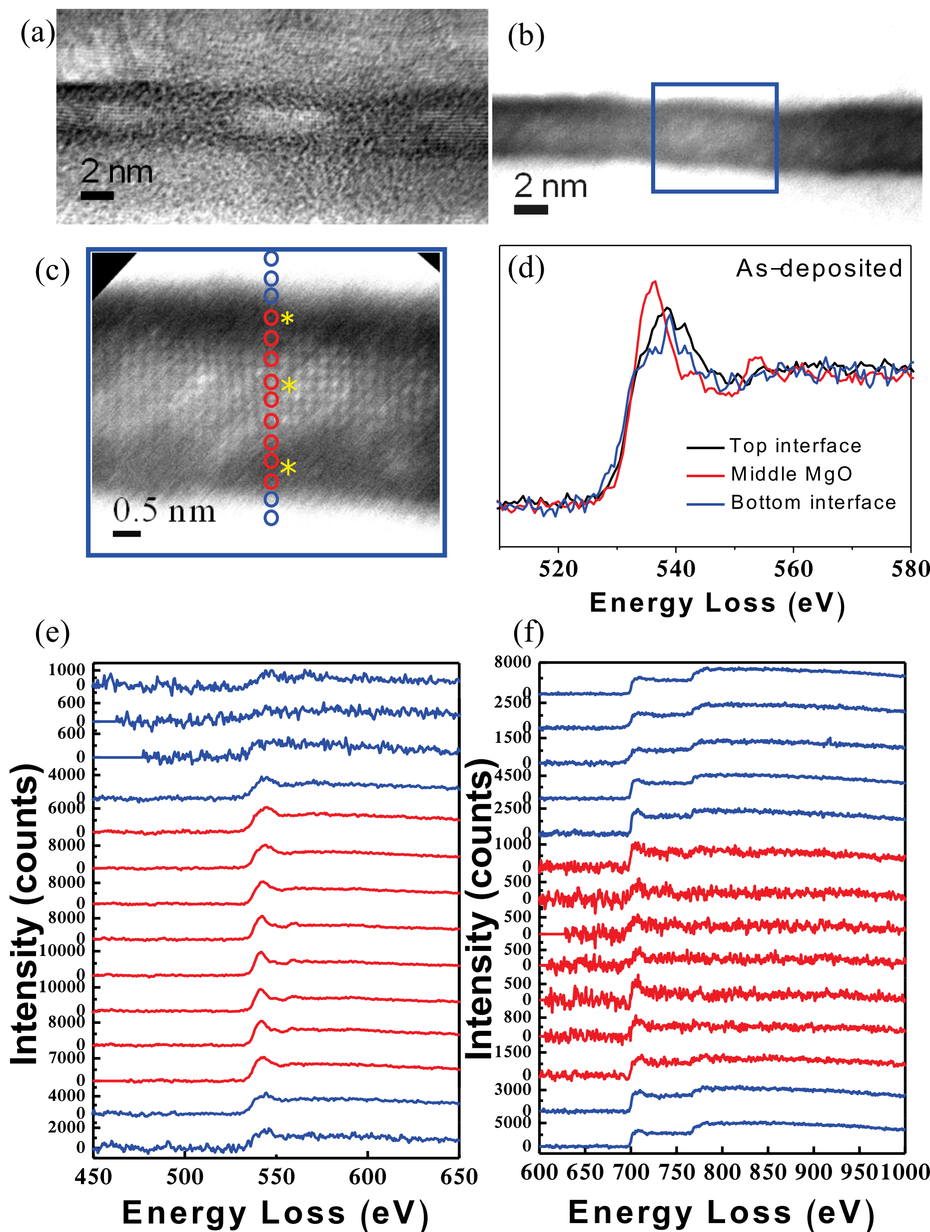

FIG. 1. Low magnification (a) MAADF and (b) HAADF STEM images of the as-deposited CoFeB/Mg + MgO/CoFeB MTJ cross section. MgO crystallites with (001) texture are observed throughout the middle of the barrier layer. (c) High magnification HAADF STEM image of a MgO crystallite from the blue rectangle in (b) confirms its (001) orientation and the disorder at the interfaces above and below it. (d) Oxygen *K*-edge electron energy-loss-near-edge structure (ELNES) probed at three positions across the MgO barrier marked by the asterisks (the bottom CoFeB/MgO interface; in the middle where the MgO fringes are observed; and the top MgO/CoFeB/ interface), ELNES changes (including pre-edge features at ∼530 eV) at both interfaces suggest the presence of oxygen vacancies. These edges are taken from the STEM-EELS line scan across the MgO barrier with all spectra for the O *K*-edge region shown in (e) and the Fe $L_{2,3}$ and Co $L_{2,3}$ edge spectra shown in (f).

suggest the formation of a mixed oxide because low intensity Fe $L_{2,3}$-edges are detected across the whole MgO barrier region [Fig. 1(f)]. The additional possibility of the formation of boron oxide has already been discussed but STEM-EELS did not detect any boron in the MTJ, perhaps in part because the thickness of the TEM cross-section (ca. 50 nm) resulted in a steep background contribution around the boron *K*-edge, resulting in relatively poor spectral sensitivity to this element. We note however that a B_2O_3 phase is the most thermodynamically favorable reaction with an enthalpy of formation of −1194.3 kJ/mol, compared to that for FeO, Fe_2O_3, Fe_3O_4, Co_3O_4, and MgO, of −251.4, −742.2, −1,015.4, −774, and −596.3 kJ/mol, respectively.[19] Regardless, the formation of mixed oxides at the interface could be attributed to the presence of oxygen vacancies during the deposition of the MgO layer.[5]

Time-resolved B 1*s* XPS of a CoFeB/MgO + Mg bilayer acquired during Ar+ ion etching did detect boron and it indicates that boron oxide is distributed across the entire as-deposited, MgO barrier [Fig. 2]. Boron oxide peaks, at a binding energy (BE) of 192.5 eV, are detected in the MgO layer after etching times of 4, 6, and 8 s. A metallic boron peak, at a BE of 187 eV, is observed throughout the bilayer and it becomes the sole B 1*s* peak after 12 s etching, indicative of the MgO having been fully etched away to reveal just the CoFeB electrode by this time. Intermediate metal boride (Co_2B/Fe_2B) peaks at BE around 188 eV are evident just above the MgO/CoFeB interface (i.e., between 6 and 8 s etching). The identification of Mg in just MgO in the barrier is confirmed in the corresponding Mg 2*p* and O 1*s* depth profiles [Fig. 2].

The O 1*s* XPS depth profile peak at a BE of 531 eV can be fitted by several components, the main oxide from MgO at ∼531 eV plus a surface oxide and boron oxide component at the BE of 532.5 eV[20–22] both of which are found in every depth scan but with relatively lower intensity as the depth or etching time increases. At the etching time of 8 s, corresponding to the MgO-CoFeB interface, another oxide component at a BE of 531.5 eV is identified; this component is suspected to

[This article is copyrighted as indicated in the article. Reuse of AIP content is subject to the terms at: http://scitation.aip.org/termsconditions. Downloaded to] IP: 129.234.252.65 On: Wed, 09 Jul 2014 08:47:52

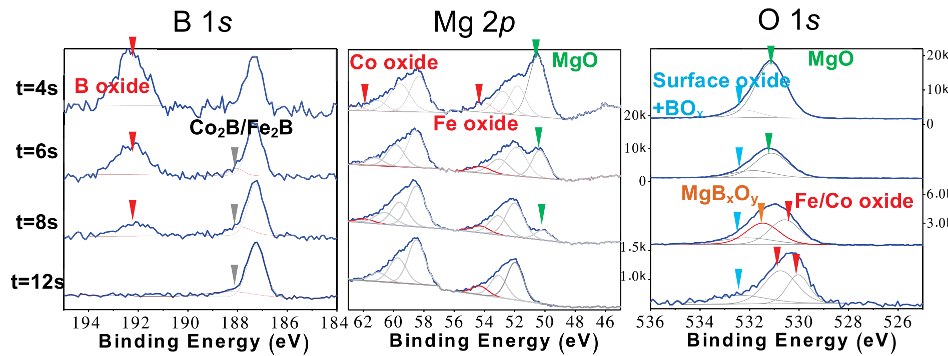

FIG. 2. XPS depth profiles of an as-deposited CoFeB/Mg + MgO bilayer: B 1*s*, Mg 2*p*, and O 1*s* spectral regions. The sets of arrows indicate phases identified by peak fitting the spectra and referencing against known binding energies for these phases, we assume the slight shifts in the binding energies of the peak maxima of each phase are due to differential charging. The spectra suggest that the CoFeB electrode has been reached after 12 s etching. MgO (at 50 eV) and boron oxide (at 192 eV) are detected in just the barrier layer, metallic boron (187 eV) is detected throughout the entire bilayer, intermediate metal boride phases at the MgO-CoFeB interface, and Fe and Co oxides across entire the junction. There is also an indication of intermixed MgB_xO_y at 531.5 eV in the O 1s spectrum at the MgO-CoFeB interface (revealed after 8 s etching).

be an intermixed MgB_xO_y previously reported by Read *et al.*[20] Oxide components at 54.7 and 61.8 eV in the Mg 2*p* spectra are present throughout the junction and are identified as Fe and Co oxides, respectively, and these phases give rise to the combined peak in the O 1*s* spectra at ∼530 eV at the MgO/CoFeB interface (t = 8 s) and the deconvolved peaks at 530.5 and 530 eV further into the CoFeB layer (t = 12 s).[23] It should be noted that at t = 12 s no MgO or BO_x are detected and so the peak in the O 1*s* spectrum at 530.5 eV has to be assigned to the transition metal oxides. It is possible that the metal oxides are present in small quantities throughout the MgO layer, as suggested by the small Fe and Co oxide components identified at low BE for all XPS etching times [Fig. 2] and the Fe $L_{2,3}$-edges detected throughout the barrier by STEM-EELS [Fig. 1(f)]. For all phase assignments, unless otherwise stated, photoelectron binding energies for reference compounds can be found in Ref. 24.

B. The annealed structure

After annealing at 375 °C, bright field STEM imaging reveals that the top CoFeB partially crystallizes into bcc CoFe with (001) texture, whereas the bottom CoFeB remains amorphous [Fig. 3(a)]. A thin, low density, amorphous layer is still visible at the bottom interface of the annealed MgO barrier particularly in the HAADF-STEM image [Fig. 3(b)]. The presence of marked changes in the main O *K*-EELS edge shape and the tentative identification of O *K*-edge prepeaks at the barrier interfaces are still evident in the EELS linescans of these annealed junctions [Fig. 3(c)], indicating the retention of vacancies and defects at both top and bottom MgO-CoFeB interfaces.

A boron EELS linescan reveals two distinctive boron states: metallic boron in the CoFeB electrodes and BO_x in the MgO barrier [Fig. 3(d)]. The B *K*-edge in the MgO barrier is characteristic of the trigonal coordination of $[BO_3]^{3-}$ in B_2O_3, which exhibits a sharp peak at ∼194 eV due to the (π*) transition and followed by a broader peak at ∼205 eV due to the (σ*) transition.[22]

The intensity of each B *K*-EEL spectrum in Fig. 3(d) is integrated over a 10 eV energy window after background subtraction and normalisation by a partial scattering cross-section, to give the B relative areal density across the barrier, as shown overlaid on the HAADF image in Fig. 3(e). The B areal density signal is higher in the bottom CoFeB electrode than the top one. It seems that the boron in the top CoFeB diffuses out of the top electrode, whereas it is retained in the bottom CoFeB electrode. A small boron signal is detected in the Ta underlayer, as has been reported before.[9,25] The detection of a higher boron content in the bottom CoFeB electrode is consistent with the inhibition of crystallization of this layer [Fig. 3(a) and Kodzuka *et al.*[15]].

On the basis that the trigonal coordination of $[BO_3]^{3-}$ is identified by STEM-EELS in the barrier of the annealed junction [Fig. 3(d)] and that the interface between the barrier and the bottom electrode remains amorphous and disordered before and after annealing [Figs. 1 and 3], it is suggested that the MgB_xO_y identified by XPS in the bilayer [Fig. 2] could actually be a $(MgO)_x(B_2O_3)_y$ mixed oxide glass. This finding is in contrast to the recent study by Rumaiz *et al.*[26] that used hard X-ray photo-electron spectroscopy (HAXPES) and near-edge X-ray absorption fine structure of CoFeB/MgO/CoFeB interfaces to show that boron migrates towards the MgO barrier and interacts with it during annealing by forming a 3-fold coordinated boron oxide compound in the MgO barrier and a 4-fold coordinated boron oxide resembling the Kotoite mineral ($Mg_3B_2O_6$) at the CoFe/MgO interface.

XPS depth profiles of an annealed bilayer sample show a similar result to that of the as-deposited bilayer [Fig. 4 compared to Fig. 2, respectively]: magnesium oxide, boron oxide, metallic borides, metallic boron, Fe and Co oxides are all detected at the same positions in the bilayers. The O 1*s* component representing the intermixed MgB_xO_y is also still detectable after annealing [red arrowed peak in the O 1*s* spectra of Fig. 4] although there could also be a MgO component to this peak as well.

Upon annealing, the low intensity interfacial regions are still visible by HAADF-STEM imaging, particularly for the bottom interface [Fig. 3(b)] and that could be due to some disorder and the boron distribution identified in the EELS linescan of the annealed barrier, i.e., there is some boron enrichment at the disordered interfaces [Fig. 3(e)]. The

[This article is copyrighted as indicated in the article. Reuse of AIP content is subject to the terms at: http://scitation.aip.org/termsconditions. Downloaded to] IP: 129.234.252.65 On: Wed, 09 Jul 2014 08:47:52

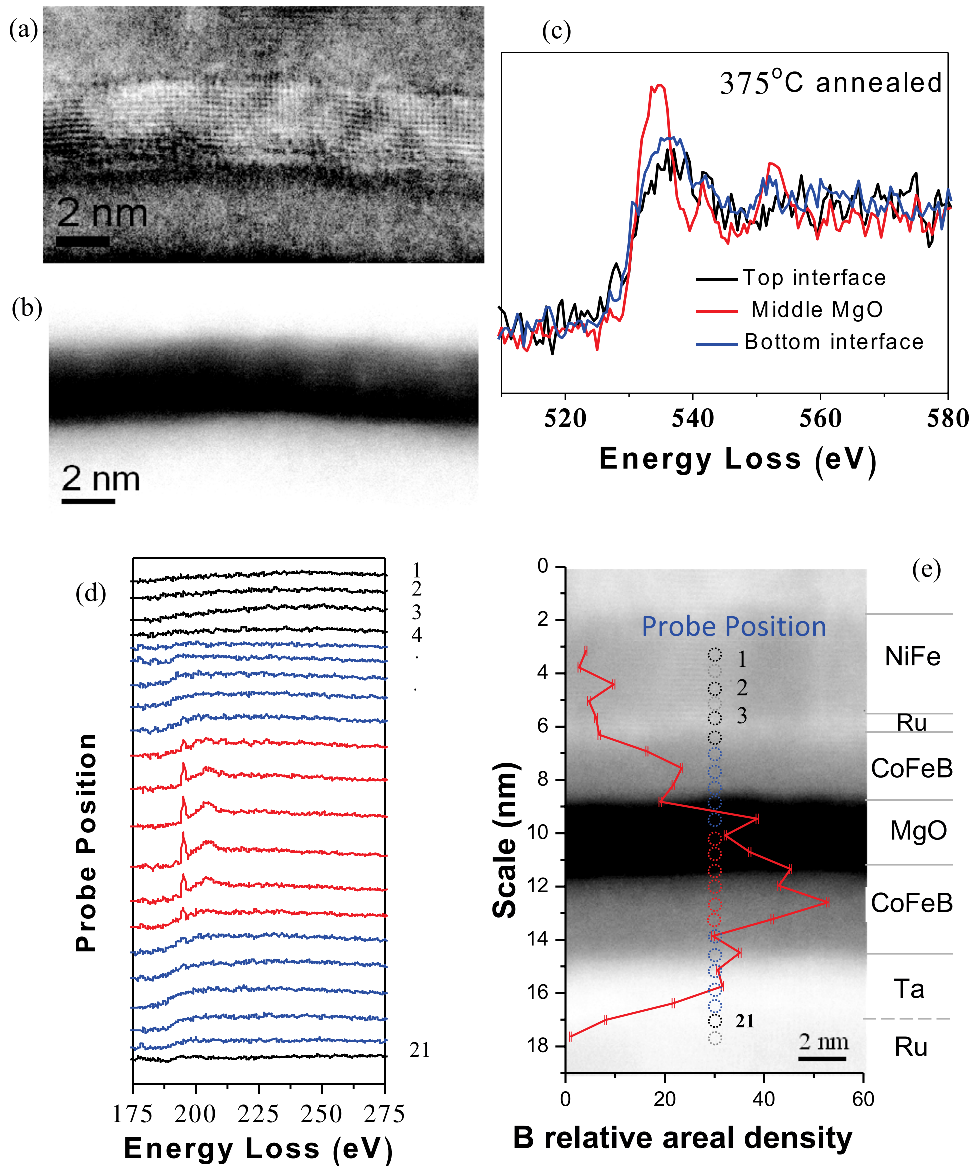

FIG. 3. STEM analysis of a cross section of the as- annealed CoFeB/Mg + MgO/CoFeB MTJ: (a) a bright field image suggests a fully crystalline MgO with (001) texture across the barrier, whilst (b) a HAADF image shows clear contrast variations across the MgO barrier, a low density amorphous layer is still retained at the bottom and, to a lesser extent, the top interfaces of the barrier. (c) Oxygen *K*-edges probed at three positions across the junction (the bottom interface of the CoFeB-MgO, in the middle of the MgO layer, and at the top MgO-CoFeB interface) still exhibit significant changes in the edge shape and the indication of edge pre-peaks at both interfaces, confirming the presence of oxygen vacancies and defects in these interfacial layers. (d) Boron *K*-edge EELS line scan across the junction with the probe positions superimposed on the associated HAADF image in (e) and the boron relative areal density also overlaid by integrating the B-edge intensity over an integration window of 10 eV after background subtraction and normalization by a partial scattering cross-section.

presence of oxygen vacancies and interstitial defects in a sub-stoichiometric MgO would enable boron to diffuse from the CoFeB electrodes potentially forming a mixed oxide glass at the interface which is presumed to be $(MgO)_x(B_2O_3)_y$. As expected, a 3-fold coordinated boron oxide compound is clearly retained in the MgO barrier upon annealing [Fig. 3(d) and Han *et al.*[14]] and because the top electrode has partially crystallized we assume some boron has diffused from this up to the B-scavenging Ta capping layer consistent with the previous work of Greer *et al.*[12] and Kodzuka *et al.*[15] One might also expect B-diffusion from the bottom electrode towards any underlying boron sinks such as Ta or Zr;[27] however, our annealing temperature is apparently not high enough for significant diffusion to have occurred into the barrier from this layer which is thicker than the top electrode, a result that is again consistent with the report of

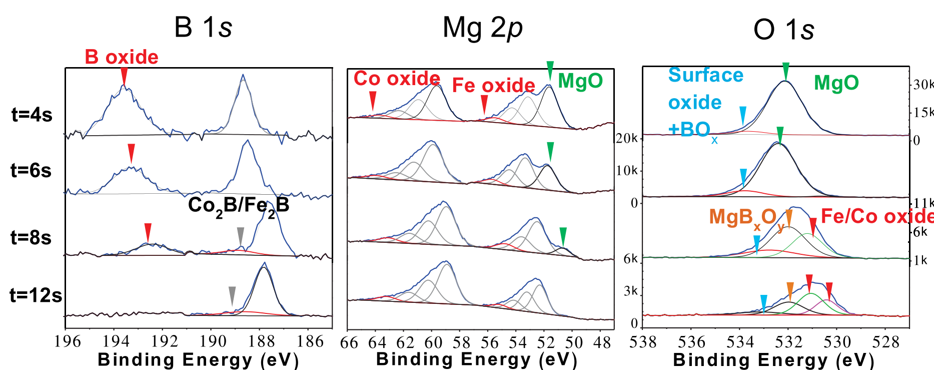

FIG. 4. XPS depth profiles of an annealed CoFeB/Mg + MgO bilayer; B 1*s*, Mg 2*p*, and O 1*s* spectral regions. All the phases identified after deposition [Fig. 2] are still present.

[This article is copyrighted as indicated in the article. Reuse of AIP content is subject to the terms at: http://scitation.aip.org/termsconditions. Downloaded to] IP: 129.234.252.65 On: Wed, 09 Jul 2014 08:47:52

Kodzuka *et al.*[15] A higher annealing temperature and/or a lower boron content of the bottom electrode are most likely required for its crystallization.

Our results show the sensitivity of HAADF-STEM imaging to compositional and structural variations at the interfaces of MTJs. Minimization of the oxidation of the bottom CoFeB electrode during the sputter deposition of MgO appears key to improving the TMR performance of these structures.

IV. CONCLUSION

We have demonstrated nanostructural characterization of a sub-stoichiometric MgO barrier in a DC-RF magnetron sputtered CoFeB/MgO based MTJ using a combination of HAADF-STEM imaging, STEM-EELS and XPS depth profile analysis. We find that the oxidation of the CoFeB electrode during the deposition of the MgO gives rise to oxidation of the surface of the electrode and the formation of defects predominantly located at the interfaces between the CoFeB and MgO layers. Correlated chemical analysis indicated that the as-deposited barrier contains a mixture of oxides including Fe and Co oxides, MgO and $(MgO)_x(B_2O_3)_y$ with a suggestion of boron enrichment at the interfaces. A similar analysis following sample annealing at 375 °C, shows improved MgO crystallinity and orientation, crystallization of bcc CoFe in the top electrode with areas of coherency across the MgO-CoFe interface plus a reduction, but not elimination, of the amorphous sub-stoichiometric layers at the interfaces and no crystallization of the thicker, bottom CoFeB electrode. Retention of a 3-fold coordinated boron oxide compound in the annealed MgO barrier is confirmed and it is suggested that a higher annealing temperature and or a lower boron content of the bottom electrode are required for its crystallization.

ACKNOWLEDGMENTS

The authors acknowledge financial support from the Engineering and Physical Sciences Research Council (EPSRC) including access to the National Facility for Aberration-corrected STEM (SuperSTEM). V.H. wishes to thank the Thai government and the Development and Promotion of Science and Technology Talented project (*DPST*) for sponsorship and support. This work has partially been supported by the Nanotechnology Center (NANOTEC), NSTDA, Ministry of Science and Technology, Thailand, through its program of Center of Excellence Network.

[1] X. G. Zhang and W. H. Butler, Phys. Rev. B **70**(17), 172407 (2004).
[2] J. Hayakawa, S. Ikeda, Y. M. Lee, F. Matsukura, and H. Ohno, Appl. Phys. Lett. **89**(23), 232510 (2006).
[3] S. Ikeda, J. Hayakawa, Y. Ashizawa, Y. M. Lee, K. Miura, H. Hasegawa, M. Tsunoda, F. Matsukura, and H. Ohno, Appl. Phys. Lett. **93**(8), 082508 (2008).
[4] S. Yuasa, T. Nagahama, A. Fukushima, Y. Suzuki, and K. Ando, Nature Mater. **3**(12), 868 (2004); J. L. Vassent, A. Marty, B. Gilles, and C. Chatillon, J. Cryst. Growth **219**(4), 444 (2000); H. L. Meyerheim, R. Popescu, N. Jedrecy, M. Vedpathak, M. Sauvage-Simkin, R. Pinchaux, B. Heinrich, and J. Kirschner, Phys. Rev. B **65**(14), 144433 (2002).
[5] J. J. Cha, J. C. Read, R. A. Buhrman, and D. A. Muller, Appl. Phys. Lett. **91**(6), 062516 (2007).
[6] V. Harnchana, A. T. Hindmarch, A. P. Brown, R. M. D. Brydson, and C. H. Marrows, J. Phys.: Conf. Ser. **241**(1), 012039 (2010).
[7] A. T. Hindmarch, V. Harnchana, D. Ciudad, E. Negusse, D. A. Arena, A. P. Brown, R. M. D. Brydson, and C. H. Marrows, Appl. Phys. Lett. **97**(25), 252502 (2010).
[8] S. V. Karthik, Y. K. Takahashi, T. Ohkubo, K. Hono, S. Ikeda, and H. Ohno, J. Appl. Phys. **106**(2), 023920 (2009).
[9] T. Miyajima, T. Ibusuki, S. Umehara, M. Sato, S. Eguchi, M. Tsukada, and Y. Kataoka, Appl. Phys. Lett. **94**(12), 122501 (2009).
[10] C. Y. You, T. Ohkubo, Y. K. Takahashi, and K. Hono, J. Appl. Phys. **104**(3), 033517 (2008).
[11] J. Y. Bae, W. C. Lim, H. J. Kim, T. D. Lee, K. W. Kim, and T. W. Kim, J. Appl. Phys. **99**(8), 08T316 (2006).
[12] A. A. Greer, A. X. Gray, S. Kanai, A. M. Kaiser, S. Ueda, Y. Yamashita, C. Bordel, G. Palsson, N. Maejima, S. H. Yang, G. Conti, K. Kobayashi, S. Ikeda, F. Matsukura, H. Ohno, C. M. Schneider, J. B. Kortright, F. Hellman, and C. S. Fadley, Appl. Phys. Lett. **101**(20), 202402 (2012).
[13] Y. Han, J. Han, H. J. Choi, H. J. Shin, and J. Hong, J. Mater. Chem. **21**(38), 14967 (2011).
[14] Y. Han, J. Han, H. J. Choi, H. J. Shin, and J. Hong, Appl. Phys. Express **5**(3), 033001 (2012).
[15] M. Kodzuka, T. Ohkubo, K. Hono, S. Ikeda, H. D. Gan, and H. Ohno, J. Appl. Phys. **111**(4), 043913 (2012).
[16] C. Wang, A. Kohn, S. G. Wang, L. Y. Chang, S. Y. Choi, A. I. Kirkland, A. K. Petford-Long, and R. C. C. Ward, Phys. Rev. B **82**(2), 024428 (2010).
[17] R. Brydson, *Aberration-Corrected Analytical Electron Microscopy* (Wiley, 2011).
[18] J. P. Velev, K. D. Belashchenko, S. S. Jaswal, and E. Y. Tsymbal, Appl. Phys. Lett. **90**(7), 072502 (2007).
[19] J. A. Dean, *Lange's Handbook of Chemistry* (McGraw-Hill, 1998).
[20] J. C. Read, P. G. Mather, and R. A. Buhrman, Appl. Phys. Lett. **90**(13), 132503 (2007).
[21] Y. Wang and M. Trenary, Chem. Mater. **5**(2), 199 (1993).
[22] H. Sauer, R. Brydson, P. N. Rowley, W. Engel, and J. M. Thomas, Ultramicroscopy **49**(1–4), 198 (1993).
[23] T. L. Barr, J. Phys. Chem. **82**(16), 1801 (1978).
[24] J. F. Moulder, W. F. Stickle, P. E. Sobol, and K. D. Bomben, *Handbook of X Ray Photoelectron Spectroscopy: A Reference Book of Standard Spectra for Identification and Interpretation of XPS Data* (Physical Electronics, reissue edition (Feb 1995), 1995).
[25] T. Ibusuki, T. Miyajima, S. Umehara, S. Eguchi, and M. Sato, Appl. Phys. Lett. **94**(6), 062509 (2009).
[26] A. K. Rumaiz, C. Jaye, J. C. Woicik, W. Wang, D. A. Fischer, J. Jordan-Sweet, and C. L. Chien, Appl. Phys. Lett. **99**(22), 222502 (2011).
[27] A. T. Hindmarch, V. Harnchana, A. S. Walton, A. P. Brown, R. M. D. Brydson, and C. H. Marrows, Appl. Phys. Express **4**, 013002 (2011).

[This article is copyrighted as indicated in the article. Reuse of AIP content is subject to the terms at: http://scitation.aip.org/termsconditions. Downloaded to] IP: 129.234.252.65 On: Wed, 09 Jul 2014 08:47:52